ADVANCED FUNCTIONAL MATERIALS
www.afm-journal.de

Tailoring the Plasmonic Modes of a Grating-Nanocube Assembly to Achieve Broadband Absorption in the Visible Spectrum

*Jeffrey Geldmeier, Tobias König, Mahmoud A. Mahmoud, Mostafa A. El-Sayed, and Vladimir V. Tsukruk**

Engineered metal-dielectric-metal nanostructures with broadband absorbing properties in the visible spectral range are fabricated by combining the plasmonic resonances of different noble metal nanostructures. Silver nanocubes and gold nanogratings couple to each other using a dielectric polymer spacer with controllable thickness, resulting in a large multiplicative enhancement of absorption properties across a broad spectral range. Narrow, long nanogrooves in a gold film are first fabricated using electron beam lithography, after which a polymer spacer layer with a controllable thickness ranging from 4 to 12 nm is assembled by spin-assisted layer-by-layer assembly. Finally, silver nanocubes with different surface coverages ranging from 12% to 22% are deposited using the Langmuir–Blodgett technique. The individual plasmon resonances of these different nanostructures are located at significantly different optical frequencies and are tuned in this study to allow a significant increase of light absorbance of the original gratings to an average value of 84% across the broad wavelength range of 450–850 nm.

1. Introduction

The excitation of free electrons forms collective plasmonic resonances in noble metal nanostructures at visible and near-IR frequencies upon exposure to incident photons, which allows the optical properties of various tailored nanostructures to be controlled in a wide wavelength range. The governing of light–matter interactions below the diffraction limit can be accomplished using nanofabrication methods such as electron-beam lithography (EBL)[1,2] or self-assembly[3,4] to incorporate plasmonic nanostructures into engineered matrices and structures. In this field, much interest has focused on obtaining light absorption at optical frequencies using plasmonic nanostructures or electromagnetic metamaterials.[5–10] These materials have a variety of applications in fields such as sensing,[11] surface enhanced Raman scattering,[12,13] light-absorbing nanowires,[14] thermal emitters,[15] thin-film photovoltaics[16] or thermophotovoltaics[17] for which efficient broadband absorption in the visible wavelength range is necessary.

However, plasmonic nanostructures are rarely able to independently achieve a broadband response due to their spectrally narrow bands that arise from their wavelength specific resonances.[18] For instance, Moreau et al. used silver nanocubes separated from a gold film by an insulating spacer to design a controlled reflectance surface that was able to achieve a maximum absorption of approximately 90% but only over a very narrow region with an approximate width of 25 nm.[6] Although impedance-matching metamaterials have been demonstrated that achieve near-perfect absorption, this absorption is not always broadband in nature and is often confined to the infrared or microwave regimes instead of the visible spectrum, although recent theoretical modeling results predict different designs with high light absorption in a controllable wavelength range.[19–23]

To achieve a very high broadband absorption in the visible spectrum, it is possible to combine multiple plasmonic resonances from different nanostructure elements in a fashion that ultimately enhances the total light absorption. For instance, Aydin et al. employed the hybridized modes of fabricated trapezoidal metallic stripes (stripes with different cross-sections) in a metal-dielectric-metal stack to achieve a broadband absorption of 71% over the 400–700 nm wavelength range.[5] Yan et al. were able to fabricate a broadband absorber in the visible spectrum with an average absorption of 95% through the use of randomly-shaped and sized gold nanoislands in another metal-dielectric-metal design.[24] Most designs focus on the incorporation of plasmonic resonances in particles[25–27] and nanoslits or nanogratings[28–31] which have been studied extensively for their unique absorption properties. Nanoparticles support localized surface plasmon resonances (LSPRs) that in addition to being angle insensitive can be an order of magnitude larger

J. Geldmeier, Dr. T. König, Prof. V. V. Tsukruk
School of Materials Science and Engineering
Georgia Institute of Technology
Atlanta, GA 30332, USA
E-mail: vladimir@mse.gatech.edu
Dr. M. A. Mahmoud, Prof. M. A. El-Sayed
School of Chemistry and Biochemistry
Georgia Institute of Technology
Atlanta, GA 30332, USA

DOI: 10.1002/adfm.201401559

© 2014 WILEY-VCH Verlag GmbH & Co. KGaA, Weinheim

than surface plasmon polaritons (SPPs) found in thin films or gratings.[26,32]

Furthermore, the near-field enhancement between two coupled nanoparticles can be several additional higher orders of magnitude compared to single particles, which is relevant for many sensing and spectroscopy techniques.[26,33] This effect is also applicable to nanoparticles separated from a plasmonic substrate by a thin dielectric layer; in this case, the nanoparticles generate mirror charge images in the substrate and the LSPRs also hybridize with SP modes, resulting in an enhanced, red-shifted resonance mode.[25] This resonance, known as the bonding mode, is symmetric in nature and oriented towards the substrate.[34] Anti-bonding modes are asymmetric in nature and oriented towards the medium but only interact with light under particular circumstances.[35,36] Small thicknesses of the spacer layer in the range of 5–20 nm have provided the strongest coupling effects and have given the best results in previous studies because resonances cannot excite well for extremely thin layers while larger layers result in poor coupling.[6,11,37]

Narrow grooves in a gold film and silver nanocubes have difference resonances that may be combined in this manner (**Figure 1**). The two different plasmonic nanostructures excite strong resonances with different spectral band positions that overlap with one another and allow a broadband absorption to be obtained. It has been demonstrated that narrow slits or grooves in noble metals can support localized standing plasmon modes.[30,38] These differ from conventional gratings which excite surface plasmon polaritons (SPPs) when the following condition is met for zero-angle incidence:

$$\lambda_{sp} = \frac{a_0}{m}\left(\frac{\varepsilon_1\varepsilon_2}{\varepsilon_1+\varepsilon_2}\right)^{\frac{1}{2}} \quad (1)$$

For SPPs excited by gratings, the resonant wavelength λ_{sp} is dependent on a number of variables, where a_o is the period of the grating, ε_1 is the dielectric constant of the medium, ε_2 is that of the metal, and m is a constant.[39] Other types of nanogratings adiabatically focus light to achieve a broadband, non-resonant absorption but are limited to low-angle incident light as well as large structure thicknesses.[40,41]

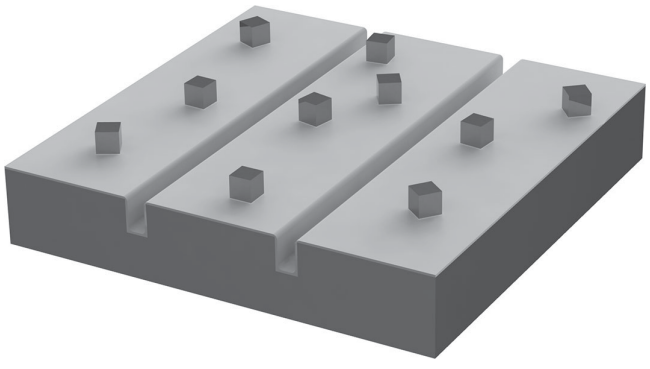

Figure 1. Silver nanocubes separated from an underlying gold nanograting by an insulating polymer spacer can be used in designing structures with broadband absorption properties.

These nanograting modes are in sharp contrast to the LSPR modes generated in small slits or grooves; in comparison to SPPs excited by conventional gratings, grooves can be considered as zero-order gratings and have relatively flat dispersion curves, leading to high absorption over a wide range of incident light angles.[31] Enhancement within these grooves scales with p/w, where p is the periodicity of the nanograting and w is the width of the grooves.[29] Nanogratings with small groove widths are attractive components for use in plasmonic absorption applications due to the ability to precisely design their structure and resulting resonances using techniques such as electron-beam lithography (EBL). However, to date little effort has been made to experimentally demonstrate how these narrow groove nanogratings and their resonances can interact with or enhance the resonances of other plasmonic nanostructures, especially in the context of mesoscale nanostructure assemblies used for broadband absorption applications.[11]

Therefore, in this study we demonstrate the use of well-defined plasmonic resonances of noble metal nanogratings and nanocubes in a constructive manner that ultimately enables the efficient, broadband absorption of light in the visible range at significantly higher levels than that possible for the individual elements. Our assembled nanostructure, presented in **Figure 2**, utilizes silver nanocubes with an edge length of 70 nm coupled to a thin gold substrate by a polymer dielectric spacer layer with a thickness of 8 nm. EBL fabrication of an underlying gold nanograting of varying widths (w) and periodicities (p) is implemented in order to achieve this high broadband absorption. Using this nanostructure design enables the plasmonic resonances of the different components at two different wavelengths to multiplicatively enhance one another, as shown in this study. A high average light absorption of 84% was achieved over the broad wavelength of 450–850 nm for p-polarized (TM) light based on the different resonances of the gold nanograting substrates and the dielectric spacer-coupled silver nanocubes.

2. Results and Discussion

2.1. Slit Modes

Gold nanogratings with groove widths of 50, 75, and 100 nm and periodicities of 350, 400, and 450 nm were fabricated with EBL in order to examine the effects of these parameters on the primary slit resonance (see Experimental Section). A height of 90 nm was chosen to maximize this resonance while avoiding the possibility of multilayers of silver nanocubes if they deposited into the grooves.

It was observed that for a constant periodicity, the primary resonance degraded and blue-shifted as the groove width was increased (**Figure 3**a). The absorption peak occurred at 770 nm for a 100 nm groove width and 709 nm for a 50 nm groove width which corresponds to a 1.2 nm blue-shift of the resonance peak wavelength per nm decrease of w (1.2 Δnm/nm). The reflectance minimum decreased from 17% to 9% as the groove width was decreased due to an increase of surface charges on the edges of the slits. The reflectance maximum at approximately 560 nm also experienced a slight decrease as

© 2014 WILEY-VCH Verlag GmbH & Co. KGaA, Weinheim

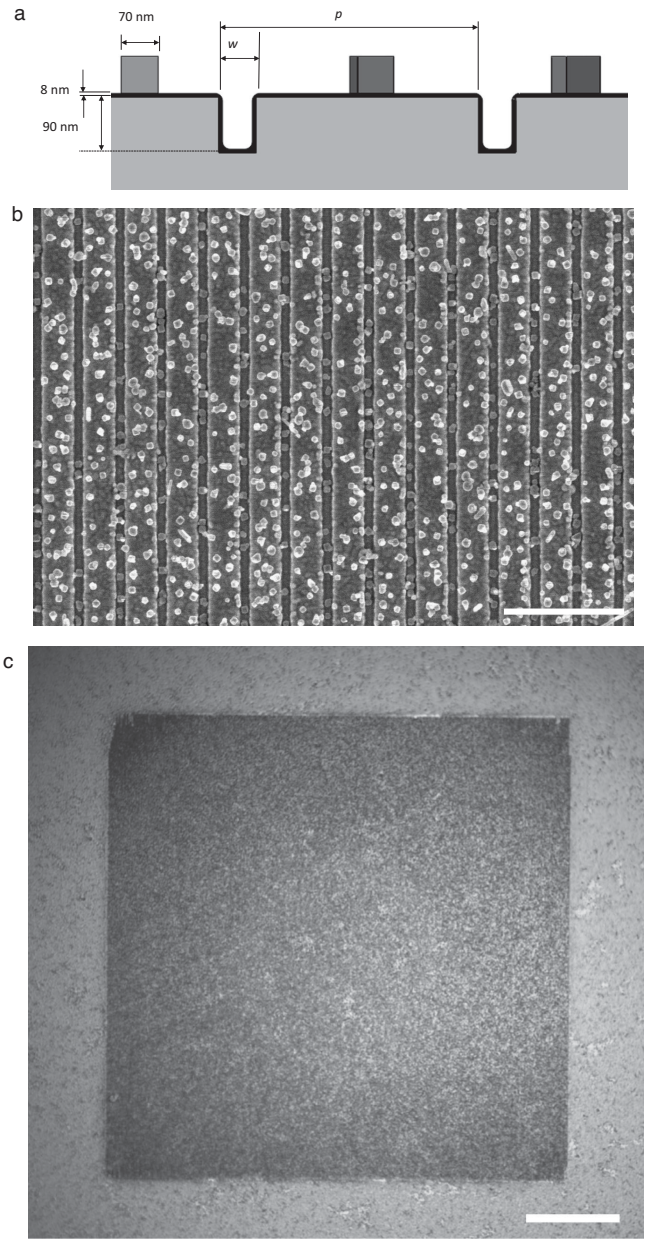

Figure 2. a) Schematic of fabricated absorber with different grating widths and periodicities. b) Scanning electron microscopy image of a fabricated grating-nanocube array with 100 nm groove widths and a 350 nm periodicity. Scale bar is 1 μm. c) Bright field microscopy image of the same array. Scale bar is 50 μm.

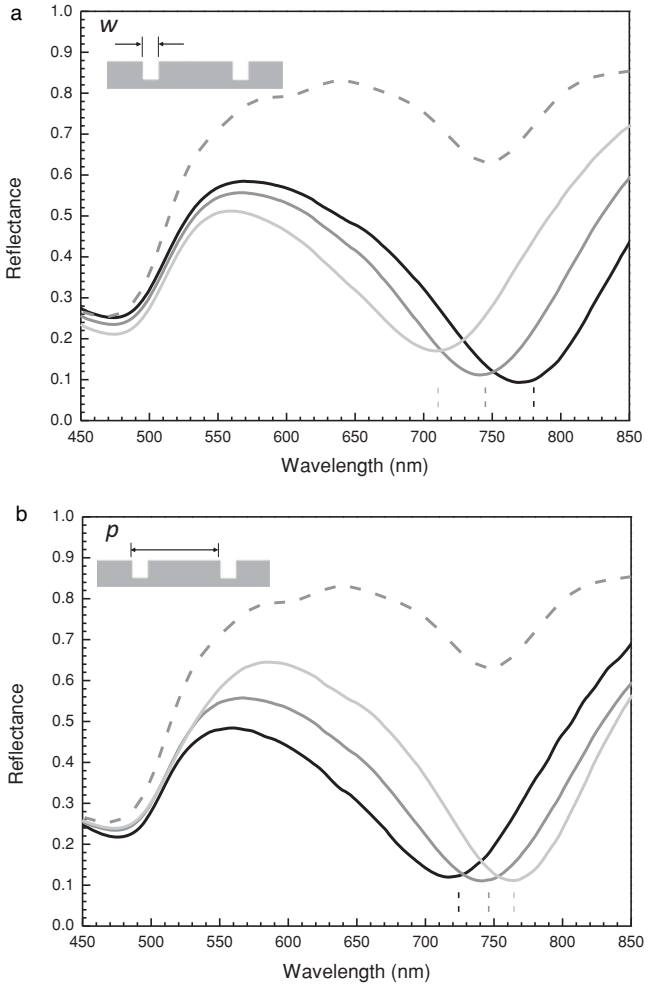

Figure 3. a) Reflectance spectra for nanogratings of a fixed p of 400 nm and a varying w of 50 nm (black), 75 nm (dark grey) and 100 nm (light grey). b) Reflectance spectra for nanogratings of a fixed w of 75 nm and a varying p of 350 nm (black), 400 nm (dark grey), and 450 nm (light grey). The dashed lines are the simulated spectra for the corresponding experimental spectra while the dashed markers indicate simulation peak positions for the respective experimental slit parameters.

the groove width was increased due to an increasing overlap with the main resonance. Keeping the groove width fixed and increasing the periodicity of the nanograting had the effect of red-shifting the resonance at a rate of 1 Δnm/nm (Figure 3b). This shift may be attributed to the individual groove modes coupling to a lesser extent with one other as the periodicity was increased. A slight decrease in the resonance was also expected due to the increase in the ratio p/w but was not experimentally observed. In all cases, the deposition of the polymer bilayers was found to red-shift the resonance mode approximately 20 nm due to the change in the local refractive index around the nanogratings (Figure S1, Supporting Information).

Finite-difference time-domain (FDTD) simulations supported the observed general trends in reflectance behavior (see Experimental Section). Reflectance minimum peak positions for simulated groove nanostructures are within 10 nm of experimental values (Figure 3). Experimental reflectance spectra were broader and had lower reflectance values than those of the simulated nanogratings, but this is could potentially be due to the imperfect periodicities and geometries as well as the finite sizes of the fabricated gratings (Figure S2, Supporting Information).

The local electric field enhancement, $|E|^2/|E_0|^2$, was plotted for the reflection minimum of two periods for each nanograting in order to visualize the plasmonic modes of the grooves (**Figure 4**). As is clear from the electric field enhancement distribution, strong coupling exists at the top corners of the grooves where the charge accumulation is the highest. On

© 2014 WILEY-VCH Verlag GmbH & Co. KGaA, Weinheim

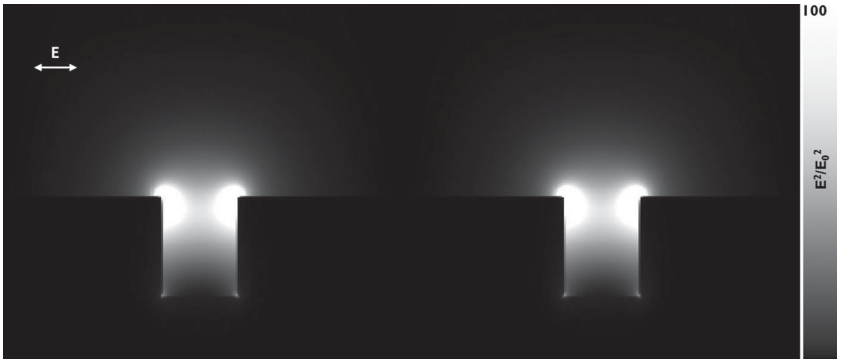

Figure 4. The electric field enhancement for a nanograting with groove widths of 50 nm and a 350 nm periodicity. A maximum enhancement of 1250 occurs at the top corners of the grooves and the enhancement has been normalized to 250 for clarity.

the other hand, little to no enhancement occurs along the outmost surface, confirming that the observed mode is local and non-propagating in nature. Such modes are also important for the angle independence absorption they exhibit.[29] This is advantageous for the broadband application being considered since SPP modes would most likely be disrupted by the sequential random deposition of nanocubes on the surface.[42]

2.2. Silver Nanocubes on a Uniform Substrate

To study the individual resonance behavior of silver nanocubes separated from a bare gold substrate, the dielectric layer thickness and the cube surface concentration were varied. A polymer dielectric thickness of 8 nm (2 bilayers) was determined to be the optimum spacer thickness for the cube surface coverages examined and resulted in the lowest reflection peak minimum values compared to the spacer thicknesses of 4 nm (1 bilayer) and 12 nm (3 bilayers) also investigated in this study.

The effects of nanocube surface coverage on the resulting reflectance properties were determined by adjusting the surface pressure during Langmuir–Blodgett (LB) deposition to 1, 2, and 4 mN m^{-1} that corresponded to different gas or liquid states on a Langmuir isotherm (**Figure 5**). The variation of surface pressure resulted in respective nanocube surface densities of 12, 15, and 22% as determined using ImageJ analysis of high contrast SEM images (see Experimental Section).

Average interparticle distances (defined as the average distance between a cube's centroid and the centroid of its nearest neighbor) were obtained using the Image Metrology SPIP software. For the surface densities of 12, 15, and 22%, average interparticle distances were respectively determined to be 134 ± 40 nm, 111 ± 42 nm, and 88 ± 34 nm. The highest surface density investigated in this study of 22% resulted in the strongest resonance and also resulted in a slight blue-shift from the spectra of lower surface densities due to increased coupling interactions between nanocubes (Figure 5).

The spacing of nanocubes in periodic FDTD simulations of both nanocube chains (1D) and nanocube square arrays (2D) was varied within the broad range to reflect a high variability in experimental surface distribution in order to analysize the experimental results. It is important to note that because the deposited nanocubes are not strictly periodic in nature, the collective response can be approximated as such provided there are multi-cube aggregates with short-range ordering that influence the spectrum. In contrast to conventional simulations of individual aggregates which cannot be practically conducted for very large surface areas with complex topography, periodic boundaries model also allows the simulation of an infinite number of nanocubes, which is more realistic for modeling a large number of particles than the modeling of isolated clusters or chains of cubes.[6,43,44]

These simulations reveal that the resonance for a 1D spacing of 300 nm between each nanocube is at 640 nm while the resonance for a 1D spacing of 120 nm is at 600 nm and is weaker, implying that the silver nanocube interparticle distance plays an important role in the observed spectral characteristics (Figure 5a). For a 2D array, an interparticle spacing of 150 nm results in the same resonance position at 600 nm (Figure S3,

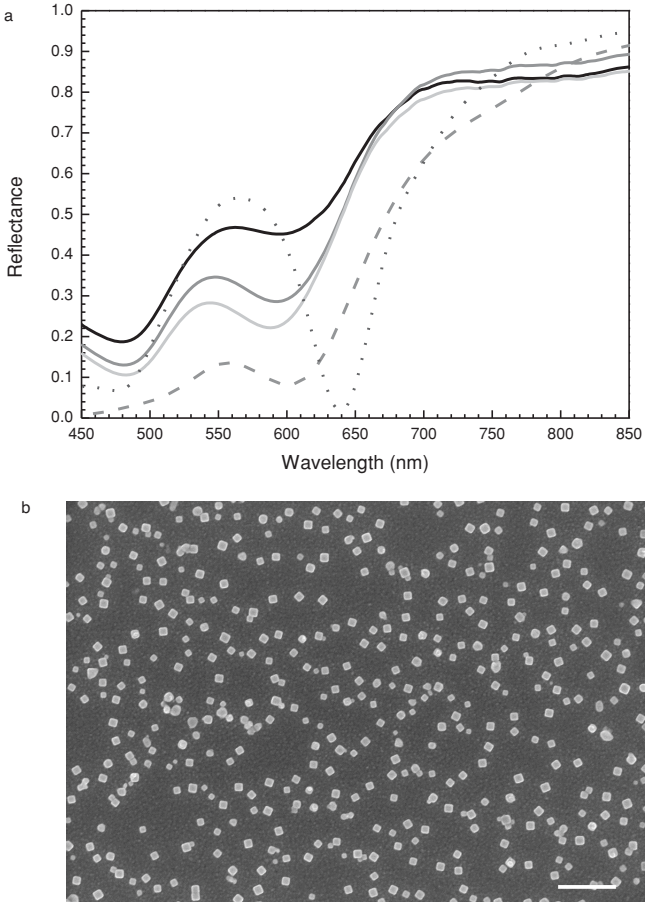

Figure 5. a) Reflectance spectra for gold substrate-coupled silver nanocubes with surface densities of 12% (black), 15% (dark grey), and 22% (light grey). The broken curves show the simulated spectra for a 1D interparticle spacing of 120 nm (dashed) and 300 nm (dotted). b) SEM image of a 15% surface coverage sample. Scale bar is 500 nm.

© 2014 WILEY-VCH Verlag GmbH & Co. KGaA, Weinheim

Supporting Information). Finally, the orientation of the cubes with respect to each other was procedurally examined to determine if it significantly altered the simulated cube resonances. These simulations confirmed that, face-to-face, face-to-edge, and edge-to-edge orientations on widely spaced nanocubes resulted in similar spectral features in contrast to the differences reported previously in literature for close-packed nanocube chains, which will be discussed later (Figure S2, Supporting Information).[44] It is important to note that neither the 1D or 2D simulations exactly replicate the complex situation of poorly ordered and widely distributed nanocubes, but they do serve as a proper model for elucidating the effect of changing the interparticle distance. The determined peak positions are also red-shifted significantly from that of silver nanocubes in a dilute solution due to the hybridization of the nanocube LSPR modes with the image charges and surface plasmons of the gold substrate, as has been documented in literature.[25]

Although coupled nanocubes display a higher reflectance minimum than that of isolated nanocubes, the associated blue-shift away from the slit modes and the resonance broadening are both beneficial for broadband absorption. The lower reflectance seen for the simulated coupled nanocubes compared to the experimental results can be attributed to the simulated nanocubes' perfect monodispersity and shape as well as their exact periodicity compared to experimentally broader distributions.

Electric field monitors for the reflectance minima peak wavelength of both 1D interparticle spacings reveal the associated plasmonic modes (**Figure 6**). As evident from these simulations, nanocubes with a 300 nm interparticle spacing are essentially isolated from their nearest neighbors and the spectrum is dominated by the nanocube-substrate bonding modes. On the other hand, both a 1D 120 nm spacing and a slightly larger 2D 150 nm spacing still exhibit a strong bonding mode but also permit weak coupling between neighboring nanocubes (Figure 6b). In both the 1D and 2D cases, changing the orientation of the cubes with respect to each other does not significantly alter the spectrum or observed modes due to the nature of the weak, long-distance coupling mode and the unaffected dominant bonding modes. In contrast, at much shorter interparticle distances, changing the orientation of the cubes would radically change the coupling mode and alter the spectrum as observed previously.[44] As a result, lower maximum field enhancements and higher reflectance peaks are ultimately present in the coupled nanocubes due to the delocalization of the electric field and the destructive interference between the nanocube bonding and coupling modes.

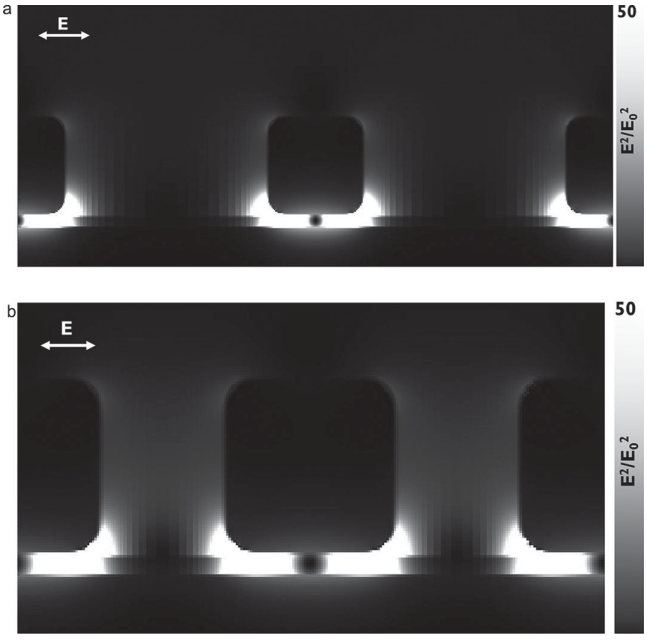

Figure 6. Electric field enhancements for a) nanocubes with an interparticle spacing of 300 nm and b) an interparticle spacing of 120 nm. Maximum theoretical enhancements of 1600 and 600 exist at the bottom corners of the cubes for the respective interparticle spacings of 300 and 120 nm, although the enhancements have been normalized to 100 for comparison between the two modes.

2.3. Grating-Nanocube Assemblies

After having separately analyzed and characterized the expected individual nanocube and nanograting modes, silver nanocubes were deposited on polymer-coated nanograting substrates (Figure 2). Because the grooves were designed to be narrow, nanocubes were expected to predominantly deposit along the top surface of the gratings. SEM images indeed confirm a high density of cubes on the top surface for all substrates, although nanocubes are also present inside grooves with larger widths (**Figure 7**a). For smaller widths, nanocubes are able to deposit on top of the grooves, resulting in an approximate 20% reduction in the grooves' visible surface area (Figure 7b).

In contrast to the trend seen for the individual nanogratings where a decrease in groove width led to a slight decrease in reflectance, the grating-nanocube assembly reflectance significantly increases as the width decreases (**Figure 8**a). This is thought to be due to the obscuration of the grooves and the alteration of their plasmonic modes by the nanocubes when they are deposited on top of nanogratings with small grooves. Even though nanocubes can deposit into grooves of larger widths, this does not appear to adversely impact the grating mode due to the localization of the resonance around the top edges of the grooves (Figure 4). The relationship between the periodicity and the nanocube-grating assembly reflectance spectra also deviated from that of the individual nanograting spectra. A clear increase in reflectance occurs with an increase of periodicity in contrast to the constant reflectance seen for the nanogratings independently, implying that the deposition of nanocubes impacts the resonance of the nanogratings which will be discussed subsequently (Figure 8b).

The overall shape of the spectrum can be generally reproduced by multiplying the individual reflectance spectra together in accordance with Beer's Law.[45] The total absorption (A) in the assembly is a product of a scalar coupling efficiency α and the individual component resonances:

$$A_{\text{tot}} = \alpha\left(A_{\text{grooves}} + A_{\text{cubes}} - A_{\text{grooves}}A_{\text{cubes}}\right) \quad (2)$$

© 2014 WILEY-VCH Verlag GmbH & Co. KGaA, Weinheim

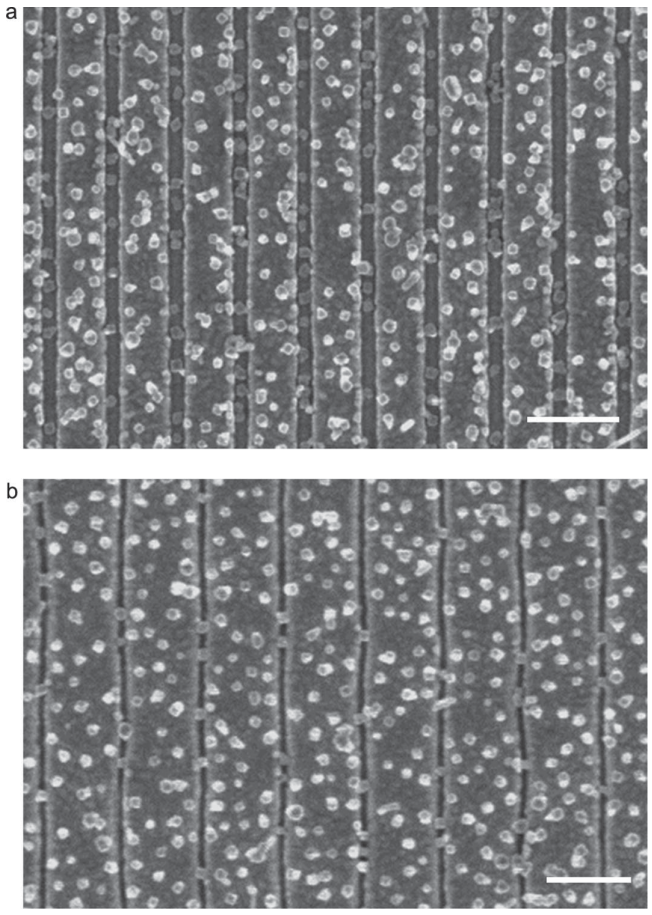

Figure 7. SEM images for 350 nm periodicity assemblies with groove widths of a) 100 nm and b) 50 nm. Scale bars are 500 nm.

Simulation of FDTD far-field power integrals of both the nanograting and the nanocube reflectance monitors reveal that <5% of reflected light is scattered outside of the far-field collection region when a numerical aperture of 0.3 is used (Figure S4, Supporting Information). This finding is in accordance with the large angle-independent absorption expected for these structures that would rarely lead to large angle scattering. This finding is also supported by previous literature results, which suggest that the absorption occurring within the structures is the dominant factor for the observed reflectance spectra.[5] If large angle scattering is therefore treated as negligible, the total reflection (R) can be expressed as:

$$R_{\text{tot}} = (1-\alpha) + \alpha R_{\text{grooves}} R_{\text{cubes}} \quad (3)$$

For perfect coupling between the nanocubes and the nanograting, the total reflection simply reduces to the multiplication of the individual resonances. The wavelength range of 450–650 nm was used to calculate the coupling efficiency as approximately 0.93 based on Equation 3 (**Figure 9**). These results suggest that less than one tenth of the total ideal resonance was eliminated through destructive interference between the separate modes, as seen by the only slight increase in reflectance when comparing the experimental and expected reflectance values below 650 nm to one another.

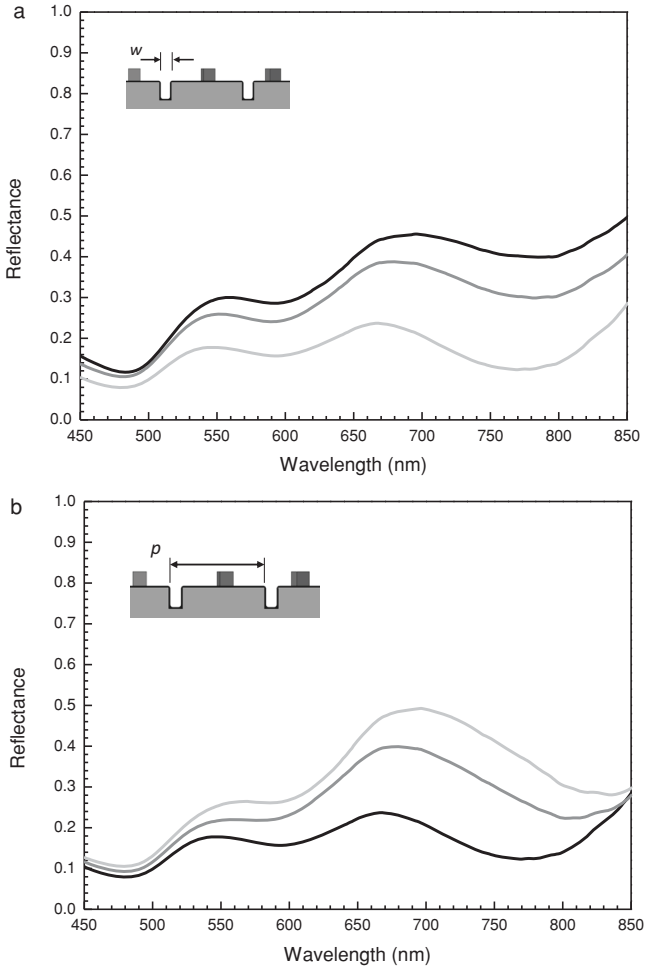

Figure 8. a) Reflectance spectra for cube-nanoslit assemblies of a fixed p of 350 nm and a varying w of 50 nm (black), 75 nm (dark grey) and 100 nm (light grey). b) Reflectance spectra for grating-nanocube assemblies of a fixed w of 100 nm and a varying p of 350 nm (black), 400 nm (dark grey), and 450 nm (light grey).

Above 650 nm, the calculated spectrum deviates from that of the experimental spectrum due to a drastic red-shift and broadening of the nanograting resonance after nanocube deposition. Further studies are needed to exactly determine what this shift is due to, as it occurs for both nanocubes deposited only along the top surface as well as for nanocubes deposited along the top surface and into the grooves. The absorption peak red-shifts even further for larger periodicities and causes the two resonance modes to effectively split, explaining the increase in reflectance associated with an increase in periodicity (Figure 8b). While this effect is not desirable for the assembly investigated in this study, it is worth noting that such splitting could be used to assist in the design of other broadband absorber assemblies or plasmonic multi-bandpass filters.

With a decreased periodicity and increased groove width leading to lower reflectance values, the largest broadband absorption of an average 84% from 450–850 nm (approximately 92% at 450 nm to 76% at 850 nm) was ultimately found for a grating-nanocube assembly with 100 nm groove widths and a 350 nm periodicity (Figure 8). Over the same wavelength

© 2014 WILEY-VCH Verlag GmbH & Co. KGaA, Weinheim

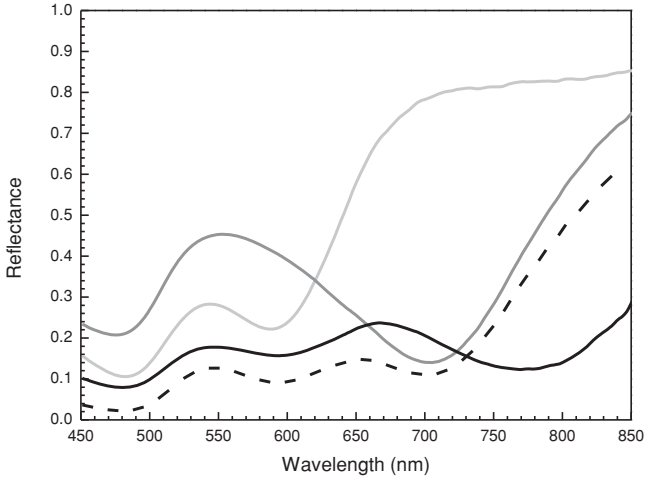

Figure 9. Reflectance spectra for the a grating-nanocube assembly with 100 nm groove widths and a 350 nm periodicity (black), the individual slit resonance (dark grey), and the individual cube resonance (light grey).The dashed curve shows the expected calculated spectrum for the cube-slit assembly with ideal coupling ($\alpha = 1$).

range, the individual components of the nanogratings and the substrate-coupled nanocubes utilized in this study have much lower respective broadband absorptions of 65% and 49%, demonstrating a synergistic enhancement between the two when they are combined in organized hybrid material structure with optimized match of their dimensions and coupling.

This materials design achieves a higher or similar broadband absorption value compared to many existing ultrathin plasmonic absorber designs and is not limited by the constraints governing impedance-matching metamaterials that make them difficult to design for broadband absorption in the visible wavelength range.[5,7,19,23,24,41] The structure fabricated in this study also contains high electromagnetic field enhancements in the polymer dielectric layer, which may potentially be substituted for an active layer for photovoltaic or other energy conversion applications.[17] Moreover, our materials design relies on a facile ambient conditions combination of patterned substrate with simple deposition on nanocubes from water surface and does not require complex shape profiling, combining multicomponent incompatible materials, or additional high temperature post-treatment. Lastly, it is worth noting that most broadband absorber designs to date use a plasmonic film or mirror to eliminate transmission and to introduce coupling effects. In contrast, the narrow slit arrays discussed in this study can be possibly integrated into many existing designs for increased absorption properties.

3. Conclusion

In conclusion, this study proves the feasibility of engineering a broadband absorber by selectively combining multiple plasmonic resonances that spectrally and spatially complement one another. We demonstrated a high level of broadband absorption in the visible range for a metal-dielectric-metal nanostructure based on the principle of constructive plasmonic resonances. In particular, this design is aided by the non-destructive overlap of two LSPRs compared to the case of combining LSPRs and periodicity-dependent SPPs which may lead to the disruption of the individual modes.[42]

In this case, silver nanocubes were separated by a gold nanoslit substrate by a thin polymer dielectric layer. The multiplicative enhancement created from these two resonances achieved a high average absorption of 84% from 450–850 nm for p-polarized light. Although this structure relies on p-polarized light to achieve high absorption, unpolarized light may be utilized instead by fabricating 2D grid structures instead of 1D grooves. Nanostructure assemblies such as this one may be useful for many optical applications in fields such as photovoltaics and thermophotovoltaics where broadband absorbance is necessary. Further enhancements to this design may be possible with the guided assembly of cubes at particular locations or the intelligent use of other overlapping, high quality resonances.

4. Experimental Section

NanoGrating Fabrication: Silicon wafers were first cleaned with Piranha solution (H_2SO_4:H_2O_2 = 3:1) for 1 h and then rinsed thoroughly with Nanopure water (18.2 MΩ cm). A 20 nm thick Ti adhesion layer was evaporated onto the substrate followed by 100 nm of Au using a CVC E-beam Evaporator in order to create a non-transparent, optically thick mirror. For the EBL resist, PMMA 950 A4 was spun at 1,800 r.p.m. to give an approximate 200 nm height and baked at 180 °C for 90 s. EBL was done using a JEOL JBX-9300FS System. After lithography, 90 nm of Au was deposited using the CVC E-beam Evaporator. Lift-off was subsequently performed using 1165 Remover for a period of 4 h, followed by a 30 s sonication step. The substrate was sequentially rinsed with acetone, methanol, and isopropanol and UV cleaned for 30 min to remove any residual resist. Due to the high aspect ratio of the developed resist, deviations from ideal line shapes were seen for nanogratings with small groove widths.

Polymer Spacer Nanolayers: Prior to bi-layer deposition, gratings were ozone etched for 1 min. in order to remove hydrocarbons and to make the surface hydrophilic. Polyallylamine hydrochloride (PAH, M_w = 60 kDA) and polystyrene sulphonate (PSS, M_w = 70 kDA) were purchased from Sigma Aldrich. LbL assembly of multilayer spacer with different thicknesses was done as described in previous experiments.[46] Briefly, 0.2 wt% solutions were prepared by dissolving the polymers in Nanopure water. Each layer was spun cast at 3000 rpm for 30 s followed by two rinse steps with Nanopure water. The thickness of each bilayer was determined to be approximately 4 nm using a spectroscopic ellipsometer (Woollam M-2000U).

LB Deposition of Silver Nanocubes: A Nima 611D trough with a water sub-layer was used for LB monolayer preparation. The surface pressure was measured with a paper Wilhelmy plate attached to a D1L-75 model pressure sensor. A 2 mL solution of silver nanocubes dispersed in chloroform was sprayed over the water surface, and the monolayer was allowed to dry for 10 min. The Langmuir monolayer was transferred to quartz or silicon substrates by the vertical dipping method at surface pressures of 1, 2, and 4 mN m^{-1}. Nanocube surface densities were analyzed using ImageJ binary thresholding of high contrast SEM images (Figure S5, Supporting Information).

Silver Nanocube Synthesis: Silver nanocubes were synthesized similarly to previously reported.[47] Silver nanocubes were prepared by ethylene glycol (EG) reduction of silver ions as follows: 75 mL of EG was heated at 140 °C and stirred in a 100 mL round bottom flask for 1 h in an oil bath. Then, 0.75 g of polyvinyl pyrrolidone (PVP, M_w = 55 kDa) dissolved in 5 mL of EG was added. The temperature of the reaction mixture was raised gradually until it reached 155 °C. Five minutes after adding PVP, 0.8 mL of 3 mM sodium sulfide in EG was added, followed by 5 mL of $AgNO_3$ solution in

© 2014 WILEY-VCH Verlag GmbH & Co. KGaA, Weinheim

EG (0.48 g dissolved in 10 mL EG). The resulting solution was stirred until it became non-transparent and the LSPR peak occurred at 474 nm. In order to prepare the nanocube solution for LB deposition, the nanocubes were cleaned of EG and excess PVP. Five mL of the nanocube solution was mixed with 10 mL deionized (DI) water and centrifuged at 10 000 rpm for 10 min. The silver nanocubes were precipitated down and re-dispersed in 10 mL of DI water. The resulting aqueous solution of nanocubes was then centrifuged at 10 000 rpm. The precipitated nanocubes were then dispersed in 0.5 mL ethanol and mixed with 1.5 mL chloroform for LB deposition.

Optical Characterization: Hyperspectral images were collected using a CytoViva Hyperspectral imaging system utilizing a diffraction grating spectrophotometer with a spectral range of 400–1000 nm and a spectral resolution of 2.8 nm. A 10× bright field objective (NA: 0.30) in reflectance mode was used to scan the surface with a 10 nm step size scan resolution. A tungsten halogen lamp with an aluminum reflector providing a wavelength range of 450–850 nm and a peak power of 150 Watts was used as a light source. P-polarized light was used to excite the nanostructures. Hyperspectral maps of the samples were normalized by a dielectric mirror with a reflectivity >99% from 350–1100 nm (Newport Corporation, 10Q20BB.HR). Approximately 3000 pixel spectra were averaged per scan to obtain each individual spectrum (Figure S6, Supporting Information). Spectra were smoothed with adjacent averaging over a 20 nm window in order to eliminate instrumentation etalon effects while still preserving all spectra features (Figure S7, Supporting Information).

Finite-Difference Time-Domain Simulations: Simulations were performed using FDTD commercial software from Lumerical Solutions, Inc. (FDTD Solutions 8.0.2). 2D simulations of three slit periods with periodic x-boundaries and perfectly matched layer (PML) y-boundaries were used for modeling the slits. 3D simulations of two cube periods with periodic x- and y-boundaries and PML z-boundaries were used for modeling the silver nanocubes. Nanocubes were modeled as both chains (periodic in x-direction) and square arrays (periodic in both x- and y-directions). Face-to-face, face-to-edge, and edge-to-edge orientations were all considered as well but show insignificant variations. Nanocubes were modeled with a 15% edge rounding, defined as the edge radius normalized by the length of the nanocube, and a 2 nm PVP coating as determined in previous studies.[48] A plane light source with a wavelength range of 300–1000 nm was used for illumination and a 1 nm mesh was used across the entire simulation region for both cubes and slits. Experimental values for gold's complex permittivity were found using ellipsometry and imported as a simulation material with a 6-coefficient fit, resulting in an RMS error of 0.153. Silver permittivity values were taken from Palik and fit with 6 coefficients, giving an RMS error of 0.150.[49]

Supporting Information

Supporting Information is available from the Wiley Online Library or from the author.

Acknowledgements

This work was supported by the U.S. Department of Energy, Office of Basic Energy Sciences, Division of Materials Sciences and Engineering under Award # DE-FG02–09ER46604.

Received: May 14, 2014
Revised: July 3, 2014
Published online: August 26, 2014

[1] S. A. Maier, M. L. Brongersma, P. G. Kik, S. Meltzer, A. A. G. Requicha, H. A. Atwater, *Adv. Mater.* **2001**, *13*, 1501.
[2] E. M. Hicks, S. Zou, G. C. Schatz, K. G. Spears, R. P. Van Duyne, L. Gunnarsson, T. Rindzevicius, B. Kasemo, M. Käll, *Nano Lett.* **2005**, *5*, 1065.
[3] T. P. Bigioni, X.-M. Lin, T. T. Nguyen, E. I. Corwin, T. A. Witten, H. M. Jaeger, *Nat. Mater.* **2006**, *5*, 265.
[4] H. Zeng, J. Li, J. P. Liu, Z. L. Wang, S. Sun, *Nature* **2002**, *420*, 395.
[5] K. Aydin, V. E. Ferry, R. M. Briggs, H. A. Atwater, *Nat. Commun.* **2011**, *2*, 517.
[6] A. Moreau, C. Ciraci, J. J. Mock, R. T. Hill, Q. Wang, B. J. Wiley, A. Chilkoti, D. R. Smith, *Nature* **2012**, *492*, 86.
[7] P. Zhu, L. Jay Guo, *Appl. Phys. Lett.* **2012**, *101*, 241116.
[8] J. Hao, J. Wang, X. Liu, W. J. Padilla, L. Zhou, M. Qiu, *Appl. Phys. Lett.* **2010**, *96*, 251104.
[9] N. Liu, M. Mesch, T. Weiss, M. Hentschel, H. Giessen, *Nano Lett.* **2010**, *10*, 2342.
[10] C. Wu, B. Neuner, G. Shvets, J. John, A. Milder, B. Zollars, S. Savoy, *Phys. Rev. B* **2011**, *84*, 075102.
[11] A. Chen, R. L. Miller, A. E. DePrince, A. Joshi-Imre, E. Shevchenko, L. E. Ocola, S. K. Gray, U. Welp, V. K. Vlasko-Vlasov, *Small* **2013**, *9*, 1939.
[12] H. Ko, S. Singamaneni, V. V. Tsukruk, *Small* **2008**, *4*, 1576.
[13] S. Chang, H. Ko, R. Gunawidjaja, V. V. Tsukruk, *J. Phys. Chem. C* **2011**, *115*, 4387.
[14] R. Gunawidjaja, S. Peleshanko, H. Ko, V. V. Tsukruk, *Adv. Mater.* **2008**, *20*, 1544.
[15] M. Laroche, R. Carminati, J.-J. Greffet, *J. Appl. Phys.* **2006**, *100*, 063704.
[16] R. A. Pala, J. White, E. Barnard, J. Liu, M. L. Brongersma, *Adv. Mater.* **2009**, *21*, 3504.
[17] H. A. Atwater, A. Polman, *Nat. Mater.* **2010**, *9*, 205.
[18] M. Rycenga, C. M. Cobley, J. Zeng, W. Li, C. H. Moran, Q. Zhang, D. Qin, Y. Xia, *Chem. Rev.* **2011**, *111*, 3669.
[19] W. Ma, Y. Wen, X. Yu, *Opt. Express* **2013**, *21*, 30724.
[20] R. Feng, W. Ding, L. Liu, L. Chen, J. Qiu, G. Chen, *Opt. Express* **2014**, *22*, A335.
[21] Q. Feng, M. Pu, C. Hu, X. Luo, *Opt. Lett.* **2012**, *37*, 2133.
[22] J. W. Park, P. Van Tuong, J. Y. Rhee, K. W. Kim, W. H. Jang, E. H. Choi, L. Y. Chen, Y. Lee, *Opt. Express* **2013**, *21*, 9691.
[23] T. Cao, C.-w. Wei, R. E. Simpson, L. Zhang, M. J. Cryan, *Sci. Rep.* **2014**, *4*, 3955.
[24] M. Yan, J. Dai, M. Qiu, *J. Opt.* **2014**, *16*, 025002.
[25] N. J. Halas, S. Lal, W.-S. Chang, S. Link, P. Nordlander, *Chem. Rev.* **2011**, *111*, 3913.
[26] M. Pelton, J. Aizpurua, G. Bryant, *Laser Photonics Rev.* **2008**, *2*, 136.
[27] R. Kodiyath, S. T. Malak, Z. A. Combs, T. Koenig, M. A. Mahmoud, M. A. El-Sayed, V. V. Tsukruk, *J. Mater. Chem. A* **2013**, *1*, 2777.
[28] A. Dhawan, M. Canva, T. Vo-Dinh, *Opt. Express* **2011**, *19*, 787.
[29] F. J. García-Vidal, L. Martín-Moreno, *Phys. Rev. B* **2002**, *66*, 155412.
[30] K.-L. Lee, S.-H. Wu, P.-K. Wei, *Opt. Express* **2009**, *17*, 23104.
[31] M. B. Sobnack, W. C. Tan, N. P. Wanstall, T. W. Preist, J. R. Sambles, *Phys. Rev. Lett.* **1998**, *80*, 5667.
[32] K. L. Kelly, E. Coronado, L. L. Zhao, G. C. Schatz, *J. Phys. Chem. B* **2002**, *107*, 668.
[33] W. Rechberger, *Opt. Commun.* **2003**, *220*, 137.
[34] L. J. Sherry, S.-H. Chang, G. C. Schatz, R. P. Van Duyne, B. J. Wiley, Y. Xia, *Nano Lett.* **2005**, *5*, 2034.
[35] Y. Jian, D. Pol Van, L. Liesbet, M. Guido, B. Gustaaf, *Nanotechnology* **2009**, *20*, 465203.
[36] S. Zhang, K. Bao, N. J. Halas, H. Xu, P. Nordlander, *Nano Lett.* **2011**, *11*, 1657.
[37] R. Alaee, C. Menzel, U. Huebner, E. Pshenay-Severin, S. Bin Hasan, T. Pertsch, C. Rockstuhl, F. Lederer, *Nano Lett.* **2013**, *13*, 3482.
[38] R. Gordon, *Phys. Rev. B* **2006**, *73*, 153405.
[39] H. F. Ghaemi, T. Thio, D. E. Grupp, T. W. Ebbesen, H. J. Lezec, *Phys. Rev. B* **1998**, *58*, 6779.
[40] D. F. P. Pile, D. K. Gramotnev, *App. Phys. Lett.* **2006**, *89*, 041111.

© 2014 WILEY-VCH Verlag GmbH & Co. KGaA, Weinheim

[41] T. Sondergaard, S. M. Novikov, T. Holmgaard, R. L. Eriksen, J. Beermann, Z. Han, K. Pedersen, S. I. Bozhevolnyi, *Nat. Commun.* **2012**, *3*, 969.
[42] J. M. Montgomery, A. Imre, U. Welp, V. Vlasko-Vlasov, S. K. Gray, *Opt. Express* **2009**, *17*, 8669.
[43] M. Toma, K. Toma, K. Michioka, Y. Ikezoe, D. Obara, K. Okamoto, K. Tamada, *Phys. Chem. Chem. Phys.* **2011**, *13*, 7459.
[44] B. Gao, G. Arya, A. R. Tao, *Nat. Nanotechnol.* **2012**, *7*, 433.
[45] J. D. Ingle, S. R. Crouch. *Spectrochemical Analysis*, PrenticeHall, Englewood Cliffs, NJ **1988**.
[46] C. Jiang, V. V. Tsukruk, *Adv. Mater.* **2006**, *18*, 829.
[47] M. A. Mahmoud, C. E. Tabor, M. A. El-Sayed, *J. Phys. Chem. C* **2009**, *113*, 5493.
[48] T. König, R. Kodiyath, Z. A. Combs, M. A. Mahmoud, M. A. El-Sayed, V. V. Tsukruk, *Part. Part. Syst. Charact.* **2014**, *31*, 274.
[49] E. D. Palik. *Handbook of Optical Constants of Solids*, Academic Press, San Diego, CA **1998**.

© 2014 WILEY-VCH Verlag GmbH & Co. KGaA, Weinheim